JOURNAL OF AIRCRAFT
Vol. 48, No. 3, May–June 2011

Stress Intensity Factor Solution for Cracks at an Offset Loaded Fastener Hole

Yan Bombardier* and Min Liao†
National Research Council Canada, Ottawa, Ontario K1A 0R6, Canada

DOI: 10.2514/1.C031127

An approximated stress intensity factor solution was obtained for radial and diametrical cracks at an offset (noncentered) loaded fastener hole. The new closed-form solution was derived by superposing and compounding several stress intensity factor solutions, including a new key stress intensity factor solution developed for cracks in a finite plate with in-plane bending loads. The accuracy of the new closed-form solutions was verified for various configurations against results found in the literature as well as finite element analysis results.

Nomenclature

a_i	=	length of crack i from the edge of the hole to the tip
a_0	=	half crack length from tip to tip
B	=	edge distance of the hole
b	=	distance between the edge and the center of the crack
D	=	diameter of the hole
e	=	fastener load eccentricity (distance between the plate centerline and the hole center)
K_i^j	=	stress intensity factor at crack i of solution j
M	=	moment caused by the offset fastener load, Pe
P	=	fastener load
R	=	radius of the hole
t	=	thickness of the panel
W	=	width of the panel
β_i^j	=	stress intensity geometric correction factor at crack i of solution j, $K_i^j/\sigma_{\text{bypass}}\sqrt{\pi a_i}$
σ_{bypass}	=	bypass stress
σ_{bearing}	=	bearing stress, P/Dt
σ'_{bearing}	=	counteracting stress due to the fastener load, applied over the plate cross section, P/Wt

I. Introduction

QUANTITATIVE risk assessment (QRA) is now required by most military aircraft structural integrity programs. A key component of QRA is generating crack growth curves for various fracture mechanics modeling scenarios, including multiple-site damage (MSD). A straightforward method for determining the probability of failure is to perform a Monte Carlo simulation that involves carrying out multiple (e.g., 10^6) deterministic fracture mechanics analyses with random initial parameters (initial crack lengths, material properties, maximum stress, etc.). A simple calculation shows that performing 10^6 simulations at 10 min per simulation would require 19 years of computational time on a computer with a single processor, which is prohibitive. Therefore, computation of accurate stress intensity factors for MSD problems must be sufficiently fast to keep the computational time to a manageable level. For this reason, numerical approaches involving direct computation using boundary and finite element methods are generally excluded in favor of closed-form and/or tabular solutions.

A common MSD cracking scenario in a lower wing panel can involve unequal cracks at an offset (noncentered) loaded fastener hole, as illustrated in Fig. 1. A closed-form solution exists for radial crack problems [1,2], but no closed-form solution is available for unequal diametrical cracks at an offset loaded hole, despite the fact that it is a common problem. In this paper, a new approximated stress intensity factor solution was developed for radial and unequal diametrical cracks at an offset loaded hole in a finite plate, with the aim of facilitating crack growth analyses of MSD scenarios. The approximated solution is presented and the accuracy is evaluated by comparing the normalized stress intensity factor solution with finite element analysis (FEA) results and the available closed-form solutions for radial cracks at an offset hole and equal diametrical cracks at a centered hole.

II. Formulation and Method of Solution

Consider the finite plate shown in Fig. 2 with an arbitrary offset fastener hole from which radial or diametrical fatigue cracks nucleate. The cyclic loading is a combination of bypass stress (σ_{bypass}) and fastener load (P).

The stress intensity factors resulting from such configurations were calculated using the principle of superposition as schematically presented in Fig. 3. The superposition method [3] is used to combine the effect of multiple loading on the stress field around the crack tip by linearly adding the stress intensity factors due to each loading. The superposition method is valid for linear problems and only for structural elements with an identical geometry and boundary conditions. The stress intensity factors for cracks at an offset loaded fastener hole (solution C) was obtained by summing the stress intensity factors caused by the bypass stress (solution A) and the bearing stress (solution B). Solutions A and B were developed using the superposition and compounding methods. The compounding method [4] is a simple and effective method used to combine the effect of several boundaries (e.g., holes, plate edges, other cracks, etc.) to solve complex geometric problems. Width (W) and thickness (t) of the plate, location (B) and diameter (D) of the hole, crack lengths (a_1 and a_2) measured from the edge of the hole, and the material were identical in solutions A, B, and C.

The following sections first present the closed-form solutions developed for solutions A and B, followed by solution C. Those solutions were developed for radial and diametrical cracks simultaneously.

A. Stress Intensity Factor at Offset Fastener Hole with Bypass Stress (Solution A)

The stress intensity factor solution at an offset hole subjected to bypass stress, shown in Fig. 4, was obtained by compounding the

Presented as Paper 2010-2864 at the 51st AIAA/ASME/ASCE/AHS/ASC Structures, Structural Dynamics, and Materials Conference , Orlando, FL, 12–15 April 2010; received 4 June 2010; revision received 23 November 2010; accepted for publication 24 November 2010.

*Assistant Research Officer, Institute for Aerospace Research, Structures and Materials Performance Laboratory, Building M-14, 1200 Montreal Road; yan.bombardier@nrc-cnrc.gc.ca.

†Senior Research Officer, Institute for Aerospace Research, Structures and Materials Performance Laboratory, Building M-14, 1200 Montreal Road; min.liao@nrc-cnrc.gc.ca.

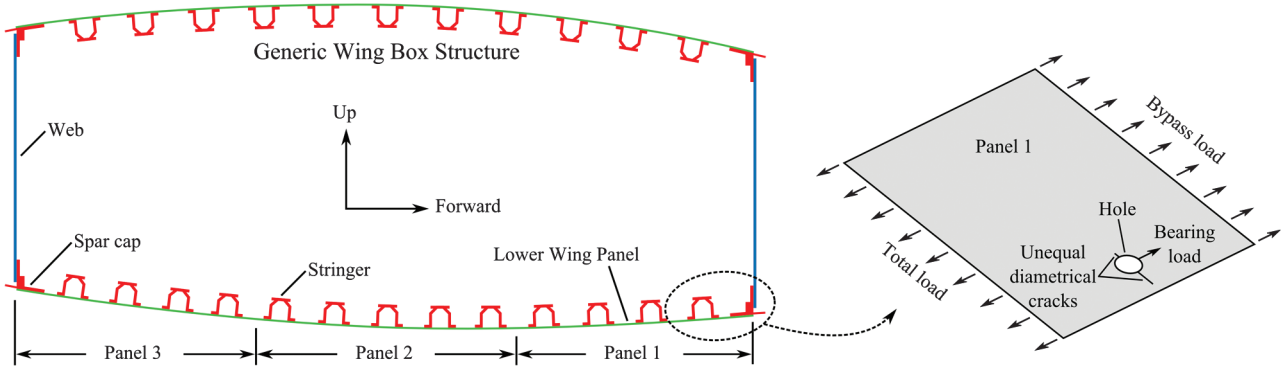

Fig. 1 Typical cracking scenario in a lower wing panel.

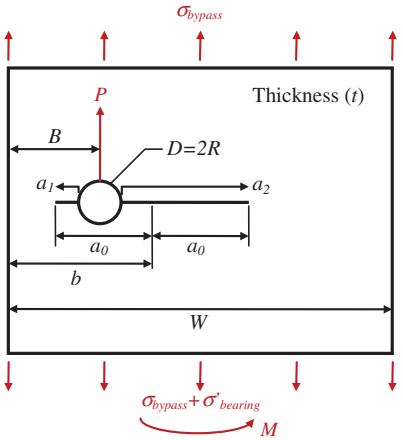

Fig. 2 Unequal diametrical cracks at an offset loaded fastener hole.

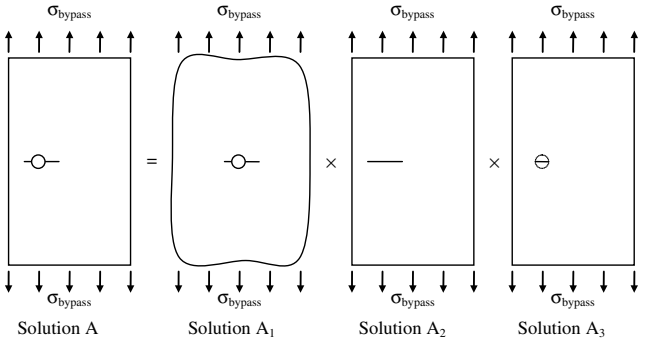

Fig. 4 Solution A developed using the compounding method.

following effects: the radial or diametrical cracks at a hole in an infinite plate (solution A_1), the edges on an offset crack in a finite plate (solution A_2), and an offset hole in a finite plate (solution A_3). All these solutions are subjected to a uniform remote bypass stress. Closed-form solutions for these subsolutions are available in the literature [3–10].

The stress intensity factor, K_i^{A}, of solution A for crack tip i is calculated as follows:

$$K_i^{\mathrm{A}} = \beta_i^{\mathrm{A}} \sigma_{\mathrm{bypass}} \sqrt{\pi a_i} \qquad i = 1, 2 \tag{1}$$

where the β factor of solution A, β_i^{A} is given by

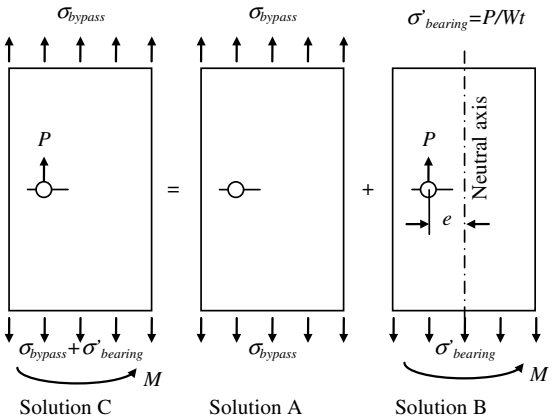

Fig. 3 Load cases superposition approach to calculate the stress intensity factor solution for diametrical cracks at an offset loaded fastener hole.

$$\beta_i^{\mathrm{A}} = \prod_{j=1}^{3} \beta_i^{\mathrm{A}_j} \tag{2}$$

In Eq. (2), the β factor of solution A_j for crack i ($i = 1$ for left crack tip and $i = 2$ for right crack tip) is given by $\beta_i^{\mathrm{A}_j}$. Note that the β factor corresponding to crack i has to be expressed in terms of the crack length measured from the edge of the hole to the tip of the crack (a_i) as illustrated in Fig. 2. σ_{bypass} is the uniformly applied bypass stress.

Solution A_1 was derived by Tweed and Rooke [10]. The β factor corresponding to a crack of length a_2, expressed in terms of the crack length to radius ratio (a_2/R), is plotted in Fig. 5 for various a_1/R ratios. The β factor corresponding to a crack of length a_1 can be easily calculated from Fig. 5 by interchanging a_1/R and a_2/R.

Although two-dimensional interpolation could be used to calculate solution A_1 from Fig. 5, a mathematical model was fitted to the results to simplify the calculations. Note that the solution for unequal diametrical cracks at a hole is also valid for radial cracks by assuming a null crack length on one of the two cracks.

Solutions A_2 and A_3 were directly taken from [5]. The β factors expressed in terms of bypass stress and crack length a_i are calculated using the following equations for $b \leq W/2$:

$$\beta_1^{\mathrm{A}_2} = \phi_1(a_0, b) \tag{3}$$

$$\beta_2^{\mathrm{A}_2} = \phi_2(a_0, b) \tag{4}$$

$$\beta_1^{\mathrm{A}_3} = \phi_1(R, B) \tag{5}$$

$$\beta_2^{\mathrm{A}_3} = \phi_2(R, B) \tag{6}$$

where

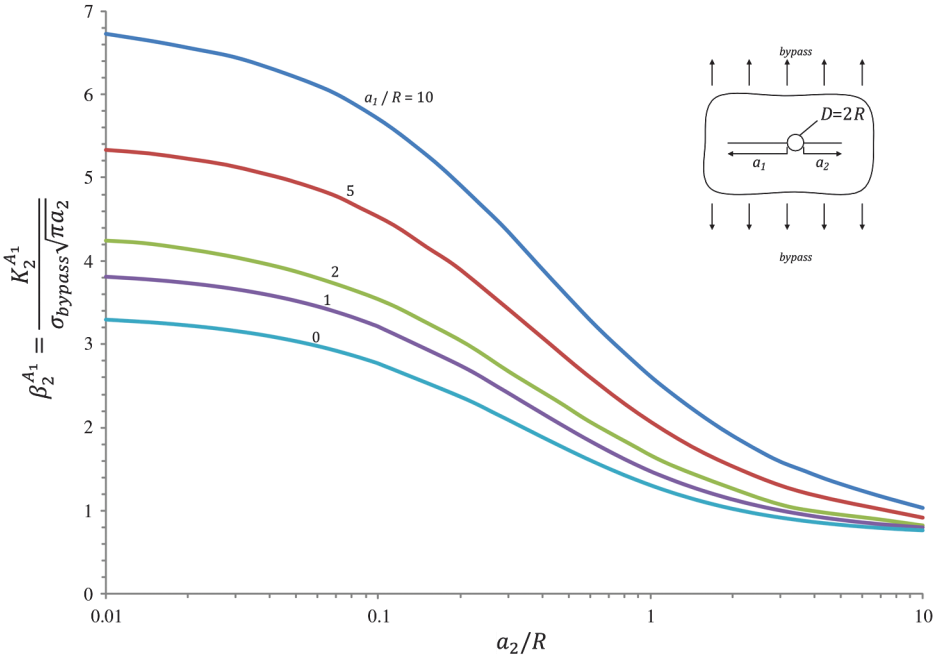

Fig. 5 β factor of solution A_1 for crack tip $i = 2$ as a function of a_1/R and a_2/R.

$$\phi_1(\alpha,\eta) = \left(\gamma + \frac{1-\gamma}{4}(1+\cos^{0.25}(\lambda_1))^2\right)\sqrt{\sec(\lambda_1)} \tag{7}$$

$$\phi_2(\alpha,\eta) = \left[1 + \left(\frac{(\sqrt{\sec(\lambda_{12})}-1)}{1+0.21\sin\left(8\arctan\left(\left(\frac{\lambda_1-\lambda_2}{\lambda_1+\lambda_2}\right)^{0.9}\right)\right)}\right)\right] \tag{8}$$

$$\lambda_1(\alpha,\eta) = \frac{\pi\alpha}{2\eta} \tag{9}$$

$$\lambda_2(\alpha,\eta) = \frac{\pi\alpha}{2W-2\eta} \tag{10}$$

$$\lambda_{12}(\alpha,\eta) = \frac{4}{7}\lambda_1 + \frac{3}{7}\lambda_2 \tag{11}$$

$$\gamma(\lambda_1,\lambda_2) = \sin\left(\frac{\pi\lambda_2}{\lambda_1+\lambda_2}\right) \tag{12}$$

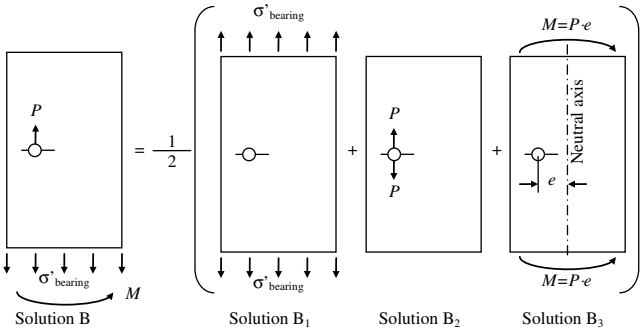

Fig. 6 Solution B developed using the superposition method.

$$a_0 = \frac{1}{2}(a_1 + a_2 + D) \tag{13}$$

$$b = B + \frac{1}{2}(a_2 - a_1) \tag{14}$$

B. Stress Intensity Factor at Offset Fastener Hole with Bearing Stress (Solution B)

Solution B was developed using the superposition method as illustrated in Fig. 6. The superposed solution includes three loading conditions that represent twice the actual applied load: the diametrical cracks at a hole in a finite plate under uniform tension caused by the bearing load (solution B_1), the splitting forces at a hole (solution B_2), and the in-plane bending caused by the load eccentricity (solution B_3). To solve this problem, symmetric loading conditions had to be assumed and solution B was therefore equal to half of the applied load. The derivation of solutions B_1, B_2, and B_3 are discussed in this section and the stress intensity factor of solution B for each crack tip, i, is calculated as follows:

$$K_i^{B} = \beta_i^{B}\sigma'_{\text{bearing}}\sqrt{\pi a_i} \tag{15}$$

Using the superposition method,

$$K_i^{B} = \frac{1}{2}\sum_{j=1}^{3} K_i^{B_j} = \frac{1}{2}\left(\sum_{j=1}^{3}\beta_i^{B_j}\right)\sigma'_{\text{bearing}}\sqrt{\pi a_i} \tag{16}$$

The β factor of solution B in Eq. (15) is therefore defined as

$$\beta_i^{B} = \frac{1}{2}\left(\sum_{j=1}^{3}\beta_i^{B_j}\right) \tag{17}$$

The β factor of solution B_1 was derived in the previous section and is equal to

$$\beta_i^{B_1} = \beta_i^{A} \tag{18}$$

The compounding strategy used for solution B_2 is illustrated in Fig. 7. This approach is based on previous work conducted for a centrally located hole [6]. Solution B_2 was developed by compounding the effects of radial or diametrical cracks at an offset hole in

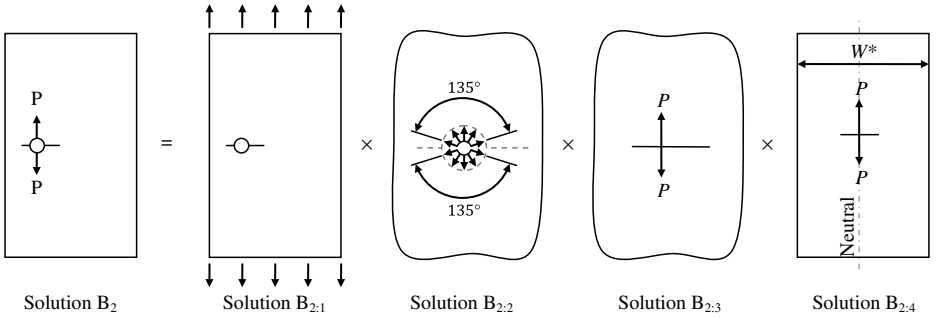

Fig. 7 Solution B_2 obtained by the compounding method.

a finite plate (solution $B_{2:1}$), the distributed splitting forces at a hole (solution $B_{2:2}$), the load asymmetry (solution $B_{2:3}$), and the edges on an offset crack in a finite plate with splitting forces on the crack surfaces (solution $B_{2:4}$). The compounded solution is given by

$$\beta_i^{B_2} = \prod_{j=1}^{4} \beta_i^{B_{2:j}} \tag{19}$$

The β factor of solution $B_{2:1}$ for crack tip i is defined using the previously developed solution:

$$\beta_i^{B_{2:1}} = \beta_i^{A} \tag{20}$$

Solution $B_{2:2}$ models distributed splitting forces at a hole with uniform load, P, providing distributed radial pressure from 22.5 to 157.5 deg and from −22.5 to −157.5 deg, as illustrated in Fig. 7. The corresponding β factor is defined as [3,11]

$$\beta_i^{B_{2:2}} = e^{0.15}(\rho^2 - 1) \tag{21}$$

where ρ is defined as

$$\rho = \frac{a_i}{a_i + R} \tag{22}$$

The β factors of solution $B_{2:3}$ are provided by the following equations for both crack tips [7]:

$$\beta_1^{B_{2:3}} = \frac{W}{\pi a_0}\sqrt{\frac{a_0 - \xi}{a_0 + \xi}} \tag{23}$$

$$\beta_2^{B_{2:3}} = \frac{W}{\pi a_0}\sqrt{\frac{a_0 + \xi}{a_0 - \xi}} \tag{24}$$

where ξ is defined as

$$\xi = \frac{1}{2}(a_1 - a_2) \tag{25}$$

Solution $B_{2:4}$ is the effect of the plate edges on the stress intensity factors induced by splitting forces on the crack surfaces. Since the in-plane bending effects are already considered by solution B_3, the model chosen for solution $B_{2:4}$ was a symmetric crack with centrally located splitting forces. The width of the plate was, however, adjusted to consider proper edge distance, yielding to an effective width, W^* shown in Fig. 7. This approach is used for an analogue problem in [5]. The β factors for solution $B_{2:4}$ are given by the following equations for $b \le W/2$, where λ_1 and λ_{12} are given in Eqs. (9) and (11):

$$\beta_1^{B_{2:4}} = \frac{\lambda_1(a_0, b)}{\sin(\lambda_1(a_0, b))} \tag{26}$$

$$\beta_2^{B_{2:4}} = \frac{\lambda_{12}(a_0, b)}{\sin(\lambda_{12}(a_0, b))} \tag{27}$$

Solution B_3, illustrated in Fig. 8, simulates the in-plane bending effect caused by the load eccentricity on an arbitrarily located crack in a finite plate. The solution was developed by compounding the effects of radial or diametrical cracks at a hole in an infinite plate (solution $B_{3:1}$) and the in-plane bending load on the arbitrarily located crack (solution $B_{3:2}$). For problems with a centrally located hole, solution B_3 is not required, as the bending moment ($M = Pe$) is zero. However, the bending effect can be significant for a panel with an offset hole. Solution B_3 is calculated using the compounding method as follows:

$$\beta_i^{B_3} = \frac{6e}{W}\prod_{j=1}^{2} \beta_i^{B_{3:j}} \tag{28}$$

The β factor of solution $B_{3:1}$ is

$$\beta_i^{B_{3:1}} = \beta_i^{A_1} \tag{29}$$

For solution $B_{3:2}$, a new correction factor was developed to properly model the effect of the induced in-plane bending. Depending on the location of the crack tips relative to the neutral axis, the in-plane bending moment may increase or decrease the stress intensity factor. As shown in Fig. 9, the crack that spreads over both sides of the neutral axis will have its stress intensity factor decreased on the compressive side and increased on the tensile side.

The problem illustrated in Fig. 9 was parameterized as a function of $\chi = (\delta - 2a_0)/W$ and $\psi = \delta/W$ and was investigated using the finite element method. Parametric two-dimensional finite element analyses were conducted using StressCheck from Engineering Software Research and Development, Inc. StressCheck uses the p-version finite method, which provides estimation of the error in energy norm as a function of the polynomial degree of the element (p level), ranging from $p = 1$ to $p = 8$. StressCheck computes the stress intensity factors using the contour integral method. To efficiently process the data, a Microsoft Excel spreadsheet interface was developed using Visual Basic for Applications to output the stress intensity factors at every crack tip as a function of the p level for each set of parameters (χ and ψ). The symmetry along the crack axis was used to reduce computational time. The StressCheck finite

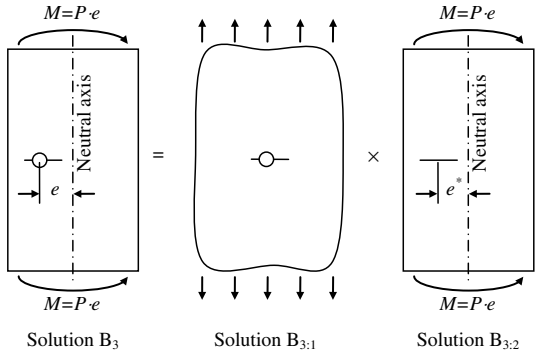

Fig. 8 Solution B_3 obtained using the compounding method.

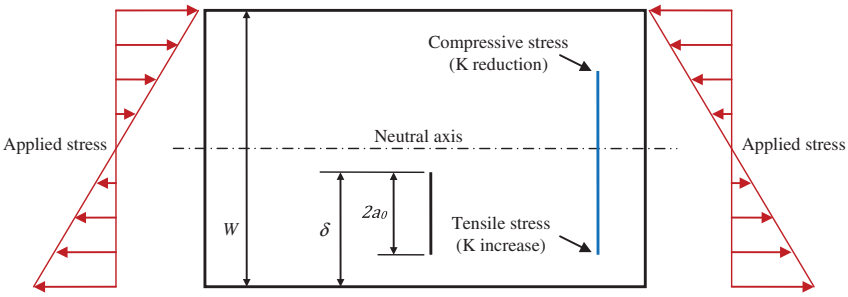

Fig. 9 Crack in a finite plate subjected to in-plane bending.

element model used for the parametric study is shown in Fig. 10 for values of $\chi = 0.25$ and $\psi = 0.50$. The model was created using triangular and quadrilateral elements p elements. Symmetric boundary conditions were applied on the lower edge, excluding the crack location. A lateral constraint was added at the lower right node to prevent rigid body motion. Linearly distributed pressure loads were applied on the top edge to simulate a unit bending moment. Mesh density was significantly increased around the crack tip to increase the accuracy of the results. The relative error, plotted in Fig. 10, was calculated for different p levels and degrees of freedom relative to the results obtained with a p level of eight. As shown, the estimated error reduces as the number of increases and the stress intensity factor converged within 0.1% at 5000 deg of freedom (p level of three) for the given parameters. All finite element analyses were conducted with a p level of eight (36,903 deg of freedom), which yielded to stress intensity factor error estimations of less than 0.3% for all data presented in this paper.

The stress intensity factors computed from the finite element analyses were converted into β factors expressed in terms of a_0 and maximum bending stress as follows:

$$\beta_i^{B_{3:2}} = \left(\frac{W^2 t}{6M}\right)\frac{K_i^{B_{3:2}}}{\sqrt{\pi a_0}} \tag{30}$$

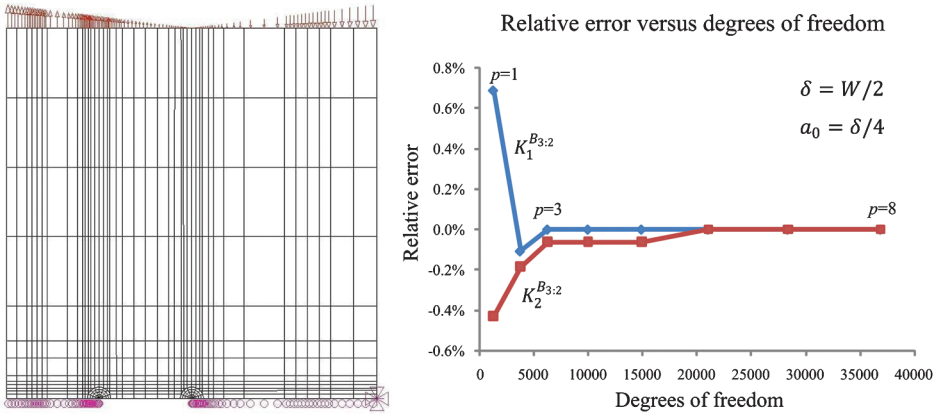

Fig. 10 StressCheck finite element model (left) and stress intensity factor convergence study (right) for $\chi = 0.25$ and $\psi = 0.50$.

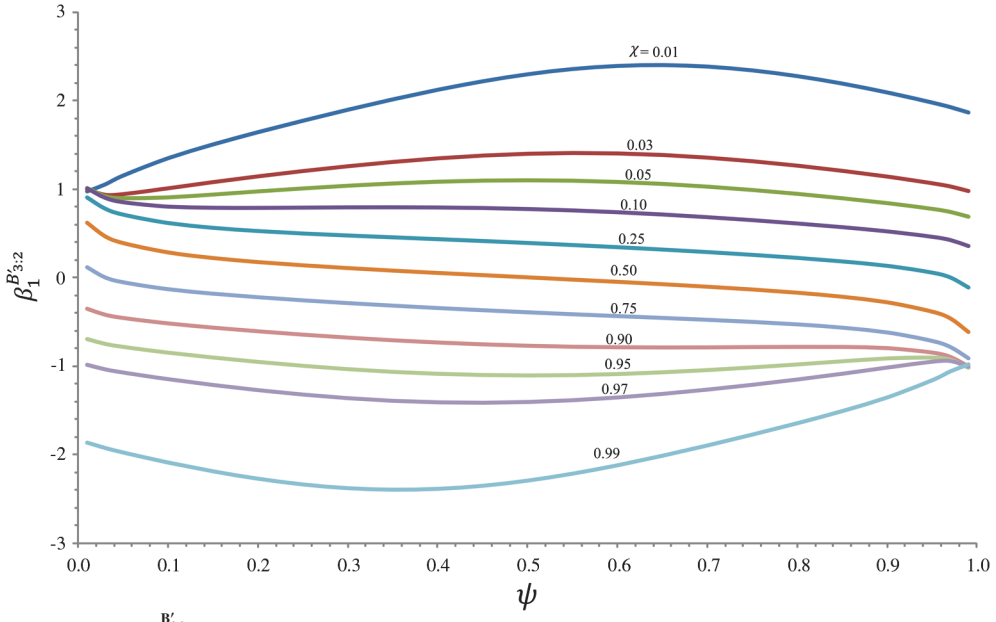

Fig. 11 β factor $\beta_1^{B'_{3:2}}$ for in-plane bending effect in a finite plate as a function of parametric dimensions χ and ψ.

Table 1 β factor $\beta_1^{B_{3:2}}$ for in-plane bending effect in a finite plate

$\psi=\delta/W$	$\chi=(\delta-2a_0)/W$											
	0.01	0.03	0.05	0.10	0.15	0.20	0.25	0.30	0.35	0.40	0.45	0.50
0.01	0.980	1.003	1.016	1.007	0.980	0.946	0.908	0.865	0.816	0.759	0.694	0.619
0.03	1.059	0.940	0.924	0.900	0.866	0.827	0.782	0.731	0.674	0.611	0.542	0.465
0.05	1.158	0.947	0.900	0.850	0.809	0.764	0.714	0.660	0.600	0.535	0.465	0.389
0.10	1.353	1.013	0.909	0.800	0.735	0.677	0.619	0.558	0.495	0.428	0.357	0.283
0.15	1.508	1.084	0.942	0.787	0.700	0.630	0.564	0.499	0.433	0.364	0.293	0.220
0.20	1.645	1.149	0.977	0.785	0.681	0.600	0.528	0.458	0.389	0.319	0.247	0.174
0.25	1.774	1.209	1.011	0.788	0.668	0.578	0.500	0.427	0.355	0.283	0.211	0.137
0.30	1.897	1.264	1.042	0.791	0.658	0.560	0.477	0.400	0.326	0.253	0.179	0.106
0.35	2.014	1.312	1.068	0.792	0.647	0.543	0.456	0.376	0.300	0.226	0.151	0.077
0.40	2.122	1.353	1.087	0.790	0.636	0.526	0.435	0.353	0.276	0.200	0.125	0.051
0.45	2.217	1.384	1.100	0.784	0.622	0.508	0.414	0.330	0.252	0.175	0.100	0.025
0.50	2.296	1.405	1.104	0.773	0.605	0.488	0.392	0.307	0.228	0.151	0.075	0.000
0.55	2.354	1.413	1.099	0.757	0.585	0.465	0.369	0.283	0.203	0.126	0.050	−0.025
0.60	2.389	1.408	1.085	0.736	0.561	0.441	0.344	0.258	0.177	0.100	0.024	−0.051
0.65	2.398	1.391	1.062	0.710	0.535	0.415	0.317	0.231	0.151	0.073	−0.003	−0.077
0.70	2.381	1.361	1.031	0.680	0.506	0.386	0.288	0.202	0.122	0.045	−0.031	−0.106
0.75	2.339	1.320	0.993	0.646	0.474	0.354	0.257	0.171	0.091	0.013	−0.063	−0.137
0.80	2.274	1.270	0.949	0.608	0.438	0.320	0.223	0.136	0.055	−0.023	−0.099	−0.174
0.85	2.190	1.211	0.899	0.566	0.399	0.280	0.183	0.095	0.013	−0.067	−0.144	−0.220
0.90	2.091	1.146	0.844	0.519	0.352	0.232	0.133	0.042	−0.044	−0.126	−0.206	−0.283
0.95	1.977	1.070	0.778	0.457	0.287	0.162	0.055	−0.043	−0.136	−0.224	−0.309	−0.389
0.97	1.927	1.034	0.743	0.420	0.245	0.114	0.000	−0.104	−0.202	−0.295	−0.383	−0.465
0.99	1.867	0.983	0.689	0.352	0.162	0.015	−0.114	−0.231	−0.340	−0.442	−0.535	−0.619

$\psi=\delta/W$	$\chi=(\delta-2a_0)/W$										
	0.55	0.60	0.65	0.70	0.75	0.80	0.85	0.90	0.95	0.97	0.99
0.01	0.535	0.442	0.340	0.231	0.114	−0.015	−0.162	−0.352	−0.689	−0.983	−1.867
0.03	0.383	0.295	0.202	0.104	0.000	−0.114	−0.245	−0.420	−0.743	−1.034	−1.927
0.05	0.309	0.224	0.136	0.043	−0.055	−0.162	−0.287	−0.457	−0.778	−1.070	−1.977
0.10	0.206	0.126	0.044	−0.042	−0.133	−0.232	−0.352	−0.519	−0.844	−1.146	−2.091
0.15	0.144	0.067	−0.013	−0.095	−0.183	−0.280	−0.399	−0.566	−0.899	−1.211	−2.190
0.20	0.099	0.023	−0.055	−0.136	−0.223	−0.320	−0.438	−0.608	−0.949	−1.270	−2.274
0.25	0.063	−0.013	−0.091	−0.171	−0.257	−0.354	−0.474	−0.646	−0.993	−1.320	−2.339
0.30	0.031	−0.045	−0.122	−0.202	−0.288	−0.386	−0.506	−0.680	−1.031	−1.361	−2.381
0.35	0.003	−0.073	−0.151	−0.231	−0.317	−0.415	−0.535	−0.710	−1.062	−1.391	−2.398
0.40	−0.024	−0.100	−0.177	−0.258	−0.344	−0.441	−0.561	−0.736	−1.085	−1.408	−2.389
0.45	−0.050	−0.126	−0.203	−0.283	−0.369	−0.465	−0.585	−0.757	−1.099	−1.413	−2.354
0.50	−0.075	−0.151	−0.228	−0.307	−0.392	−0.488	−0.605	−0.773	−1.104	−1.405	−2.296
0.55	−0.100	−0.175	−0.252	−0.330	−0.414	−0.508	−0.622	−0.784	−1.100	−1.384	−2.217
0.60	−0.125	−0.200	−0.276	−0.353	−0.435	−0.526	−0.636	−0.790	−1.087	−1.353	−2.122
0.65	−0.151	−0.226	−0.300	−0.376	−0.456	−0.543	−0.647	−0.792	−1.068	−1.312	−2.014
0.70	−0.179	−0.253	−0.326	−0.400	−0.477	−0.560	−0.658	−0.791	−1.042	−1.264	−1.897
0.75	−0.211	−0.283	−0.355	−0.427	−0.500	−0.578	−0.668	−0.788	−1.011	−1.209	−1.774
0.80	−0.247	−0.319	−0.389	−0.458	−0.528	−0.600	−0.681	−0.785	−0.977	−1.149	−1.645
0.85	−0.293	−0.364	−0.433	−0.499	−0.564	−0.630	−0.700	−0.787	−0.942	−1.084	−1.508
0.90	−0.357	−0.428	−0.495	−0.558	−0.619	−0.677	−0.735	−0.800	−0.909	−1.013	−1.353
0.95	−0.465	−0.535	−0.600	−0.660	−0.714	−0.764	−0.809	−0.850	−0.900	−0.947	−1.158
0.97	−0.542	−0.611	−0.674	−0.731	−0.782	−0.827	−0.866	−0.900	−0.924	−0.940	−1.059
0.99	−0.694	−0.759	−0.816	−0.865	−0.908	−0.946	−0.980	−1.007	−1.016	−1.003	−0.980

The β factors, $\beta_i^{B_{3:2}}$, at crack tip 1 as a function of χ and ψ are provided in Fig. 11. The tabulated values of $\beta_i^{B_{3:2}}$ including additional χ and ψ values are also given in Table 1. The correction factor for crack tip $i=2$ can be obtained by reversing the χ and ψ parameters, such that $\beta_2^{B_{3:2}}(\chi,\psi)=-\beta_1^{B_{3:2}}(\chi',\psi')$ where $\chi'=1-\psi$ and $\psi'=1-\psi$.

C. Total Stress Intensity Factor (Solution C)

The stress intensity factor for each crack tip of solution C, as illustrated in Fig. 3, is calculated as the summation of the factors due to bypass stress (solution A) and bearing stress (solution B):

$$K_i^C = K_i^A + K_i^B \tag{31}$$

Equation (31) can be expressed in terms of the β factors provided in this paper:

$$K_i^C = \beta_i^C \sigma_{bypass}\sqrt{\pi a_i} = \beta_i^A \sigma_{bypass}\sqrt{\pi a_i} + \beta_i^B \sigma'_{bearing}\sqrt{\pi a_i} \tag{32}$$

Table 2 Parametric case study for the evaluation of the closed-form solution

Identification	B/W	a_1/a_2
Radial crack		
Case 1a	0.5	$\infty(a_2=0)$
Case 1b	0.2	$\infty(a_2=0)$
Case 1c	0.8	$\infty(a_2=0)$
Equal diametrical cracks		
Case 2a	0.5	1.0
Case 2b	0.2	1.0
Case 2c	0.8	1.0
Unequal diametrical cracks		
Case 3a	0.5	4.0
Case 3b	0.2	4.0
Case 3c	0.8	4.0

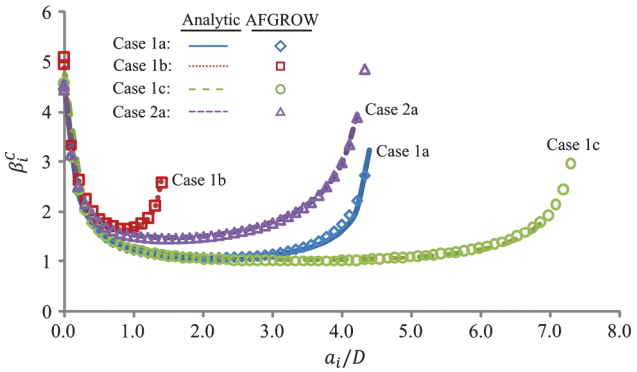

Fig. 12 Comparison of the closed-form (analytic) solution with available solution in AFGROW.

To simplify the use and flexibility of this solution, the concept of bearing-to-bypass stress ratio (BBR) was used:

$$\mathrm{BBR} = \frac{\sigma_{\mathrm{bearing}}}{\sigma_{\mathrm{bypass}}} = \frac{W}{D}\frac{\sigma'_{\mathrm{bearing}}}{\sigma_{\mathrm{bypass}}} \tag{33}$$

Equation (32) expressed in terms of bypass stress is given by

$$K_i^{\mathrm{C}} = \beta_i^{\mathrm{C}}\sigma_{\mathrm{bypass}}\sqrt{\pi a_i} = \beta_i^{\mathrm{A}}\sigma_{\mathrm{bypass}}\sqrt{\pi a_i} + \beta_i^{\mathrm{B}}\left(\frac{D}{W}\mathrm{BBR}\sigma_{\mathrm{bypass}}\right)\sqrt{\pi a_i} \tag{34}$$

where β_i^{C} can be expressed as

$$\beta_i^{\mathrm{C}} = \beta_i^{\mathrm{A}} + \beta_i^{\mathrm{B}}\left(\frac{D}{W}\mathrm{BBR}\right) \tag{35}$$

where β_i^{A} and β_i^{B} are given by Eqs. (2) and (17), respectively.

III. Numerical Results and Discussion

To demonstrate the applicability of the developed solution, nine cases were solved using the closed-form solution, the finite element method, and the "classic model" solutions available in AFGROW, whenever available. The cases include radial crack problems, equal and unequal diametrical crack problems with offset and centered holes. The tested configurations are presented in Table 2 as a function of the location of the hole, B/W, and the crack length ratio, a_1/a_2, which was assumed constant for each problem. A constant BBR of 1.0 was used for all configurations.

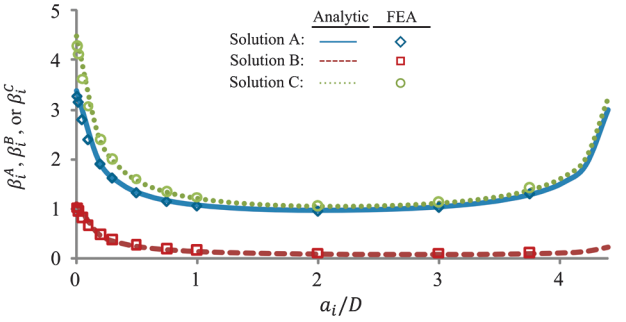

a) Case 1a: radial crack at a centrally located hole

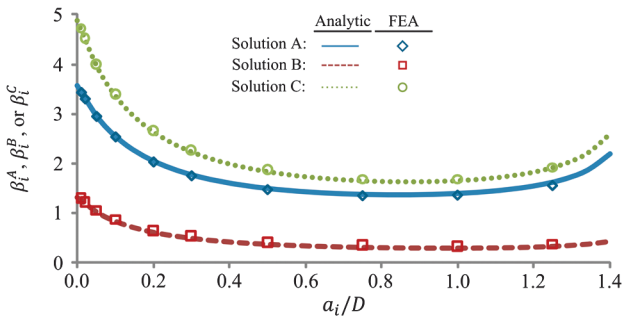

b) Case 1b: radial crack at an offset hole (crack towards closest edge)

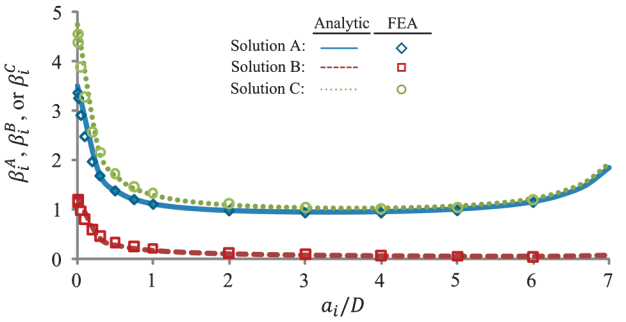

c) Case 1c: radial crack at an offset hole (crack away from closest edge)

Fig. 14 Comparison of the closed-form (analytic) solution with FEA results for cases 1a to 1c.

The first verification tests were conducted with cases 1a, 1b, 1c, and 2a. These cases were selected as the closed-form solutions are available and implemented in AFGROW. The solution provided by AFGROW for radial cracks includes correction factors determined using StressCheck, such as an additional width β factor (also used for

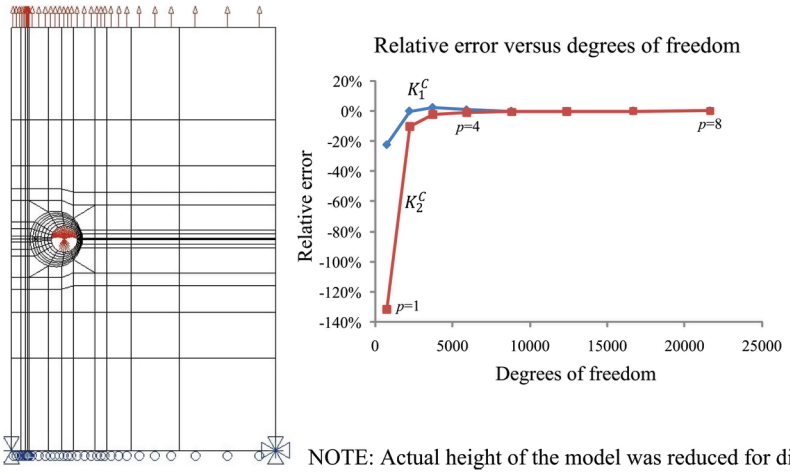

Fig. 13 StressCheck finite element model (left) and stress intensity factor convergence study of diametrical cracks at an offset loaded hole: $a_1/a_2 = 4.0$, $a_1 = 0.6$ in., $W = 10$ in., $D = 1$ in.

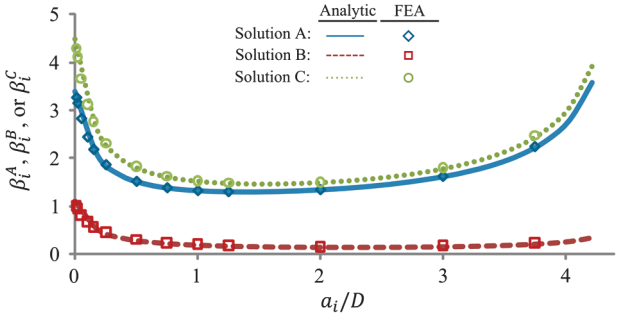

a) Case 2a: Equal diametrical cracks at a centrally located hole

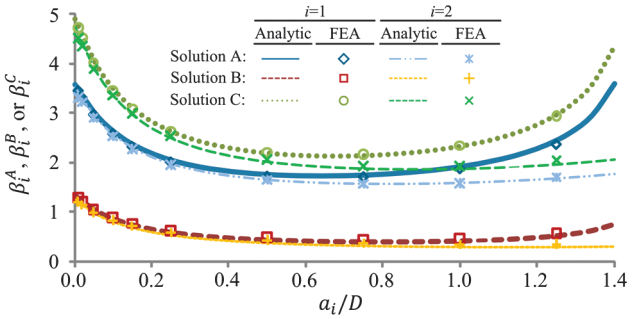

b) Case 2b: Equal diametrical cracks at an offset hole (B=2.0 inches)

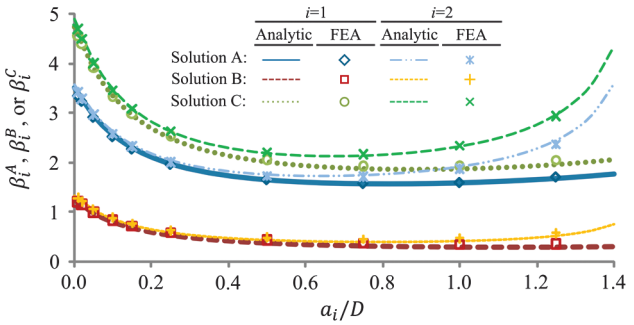

c) Case 2c: Equal diametrical cracks at an offset hole (B=8.0 inches)

Fig. 15 Comparison of the closed-form (analytic) solution with FEA results for cases 2a to 2c.

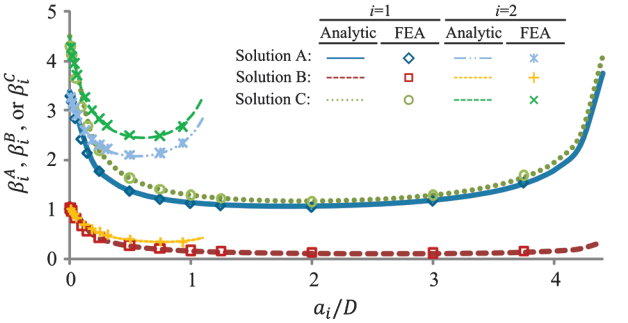

a) Case 3a: Unequal diametrical cracks (a_1/a_2=4.0) at a centrally located hole

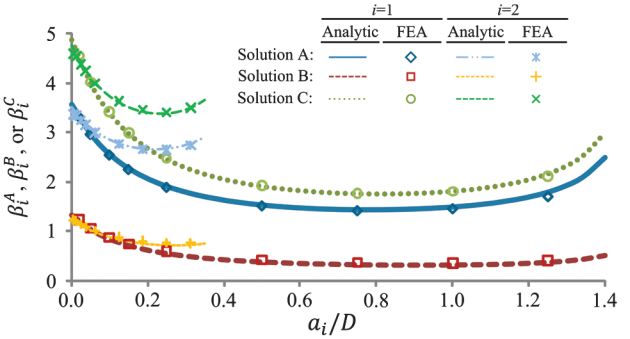

b) Case 3b: Unequal diametrical cracks (a_1/a_2=4.0) at an offset hole (B=2.0 inches)

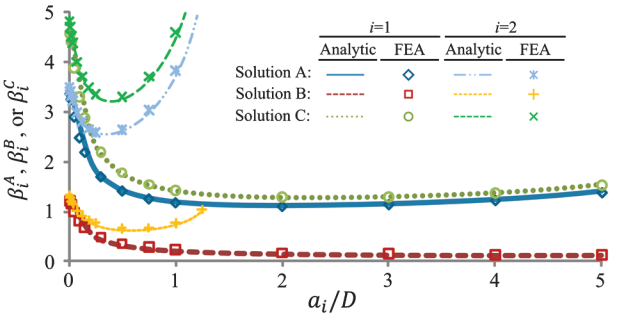

c) Case 3c: Unequal diametrical cracks (a_1/a_2=4.0) at an offset hole (B=8.0 inches)

Fig. 16 Comparison of the closed-form (analytic) solution with FEA results for cases 3a to 3c.

diametrical cracks), a bearing load β factor, and a β factor for offset holes [2]. Bypass stress was used as a stress reference for all AFGROW simulations. The β factors expressed in terms of crack length a_i and bypass stress are compared in Fig. 12 for cases 1a, 1b, 1c, and 2a under combined loading (bypass and bearing). The β factors calculated by AFGROW were marginally higher than the ones obtained using the developed solution. The results obtained using the proposed solution agreed with the results from AFGROW within 5%.

The linear static finite element analyses were conducted using StressCheck. The panel was fully modeled to simulate the asymmetric bearing load case using triangular and quadrilateral p elements. Symmetric boundary conditions were applied on the lower edge of the model. The data used for the calculations were: width of the plate, $W = 10$ in., the diameter of the hole, $D = 1$ in., and the thickness of the plate, $t = 1$ in. The hole was modeled as an open hole and bearing loads were applied with sinusoidal radial pressure distribution while uniform pressure was applied at the upper edge of the plate. The FEA results were extracted for solutions A, B, and C for close comparison with the proposed closed-form solution. The parametric finite element model is illustrated in Fig. 13.

Convergence was verified against the p level. The relative error calculated based on the results obtained at $p = 8$ is shown in Fig. 13 as a function of the number of degrees of freedom. The stress intensity factors converged within 1% with less than 6000 deg of freedom, which corresponds to a p level of four. All FEA results presented in this section were calculated with a p level of eight to ensure convergence.

The comparison of β_i^A, β_i^B, and β_i^C with the FEA results are provided in Figs. 14–16 for the nine cases presented in Table 2. The results of solution A agreed very well with the FEA results (within 3% for most crack length). For solution B, good agreement was obtained between the two solutions for small crack lengths, whereas the difference between the two solutions seemed to increase for larger crack lengths. For combined loading, however, this larger discrepancy did not significantly affect the calculated stress intensity factor of solutions C as the contribution of the bearing stress become marginal for larger crack length. Overall, good agreement was obtained between the proposed solution and the FEA results.

The contribution of in-plane bending (solution B_3) was evaluated by comparing the β factors of solution B (bearing stress) with and without the in-plane bending. Neglecting the in-plane bending effect resulted in underestimating solution B by up to 33% for the tested cases. Solution B for case 3b is plotted in Fig. 17 with and without the in-plane bending effect against the results obtained using finite element method. The stress intensity factor solution developed with the in-plane bending significantly effect significantly contributed to improve the accuracy of the closed-form solution.

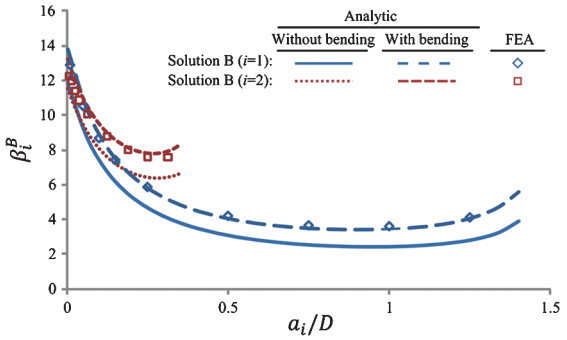

Fig. 17 Effect of in-plane bending on the β factors of solution B for case 3b.

IV. Conclusions

The closed-form solution developed in this paper enables the calculation of stress intensity factors for radial and diametrical cracks at an offset loaded hole. This solution was found to reproduce the classic model solutions available in AFGROW for radial cracks at an offset hole and equal diametrical cracks at a centrally located hole. The developed solution, however, expands the crack growth modeling capabilities to unequal diametrical cracks at an offset loaded hole. Comparison with FEA results for various configurations suggests that the solution provides accurate stress intensity factor results.

One of the key components used to develop the closed-form solution is the stress intensity solution for a center crack arbitrarily located in a finite plane with in-plane bending loads. Stress intensity factor solutions for this problem were developed using parametric finite element analyses and are provided in this paper. This solution complements the solution readily available in stress intensity factor handbooks.

The developed solutions can be very useful for damage tolerance analysis of structures and can be easily expanded to model additional effects, such as the presence of adjacent cracks, holes, or stringers, by using the compounding method.

Acknowledgments

This work was performed with financial support from Defence Research and Development Canada and the National Research Council Canada through project 13ph11 (Quantitative Risk Analysis of Aircraft Structures, under 13ph: Economic Life Assessment for Canadian Forces Air Fleets) and other contracts with the Department of National Defence of Canada. The authors would like to thank Yajun Guo for reviewing this work and providing results that contributed to improve the accuracy of the closed-form solution.

References

[1] Harter, J. A., "An Alternate Closed-Form Stress Intensity Solution for Single Part-Through and Through-the-Thickness Cracks at Offset Holes," Air Force Research Labs. Rept. AFRL-VA-WP-TR-1999-3001, 1998.

[2] Harter, J. A., "AFGROW User Guide and Technical Manual (AFGROW for Windows 2K/XP, version 4.0012.15)," Air Force Research Labs. Rept. AFRL-VA-WP-TR-2008-XXXX, 2008.

[3] Gallagher, J. P., Giessler, F. J., Berens, A. P., and Engle, R. M. Jr., "USAF Damage Tolerant Design Handbook: Guidelines for the Analysis and Design of Damage Tolerant Aircraft Structures," Air Force Wright Aeronautical Labs. Rept. AFWAL-TR-82-3073, 1984.

[4] Rooke, D. P., *Compounding Stress Intensity Factors: Applications to Engineering Structures*, Parthenon, Carnforth, Lancashire, England, U.K., 1986, chaps. 3–4, 6.

[5] Miedlar, P. C., Berens, A. P., Gunderson, A., and Gallagher, J. P., "USAF Damage Tolerant Design Handbook: Guidelines for the Analysis and Design of Damage Tolerant Aircraft Structures," Air Force Research Labs. Rept. AFRL-VA-WP-TR-2003-3002, 2002.

[6] Kathiresan, K., Hsu, T. M., and Brussat, T. R., "Advanced Life Analysis Methods: Crack Growth Analysis Methods for Attachment Lugs," Air Force Wright Aeronautical Labs. Rept. AFWAL-TR-84-3080, Vol. 2, Marietta, GA, 1984.

[7] Tada, H., Paris, P. C., and Irwin, G. R., *The Stress Analysis of Cracks Handbook*, 2nd ed., Paris Productions, St. Louis, MO, 1985, pp. 2.22, 5.10.

[8] Murakami, Y., *Stress Intensity Factors Handbook*, 1st ed., Pergamon, Oxford, 1987, Chaps. 2, 4, 5.

[9] Rooke, D. P., and Cartwright, D. J., *Compendium of Stress Intensity Factors*, H.M.S.O, London, 1976, chap. 1.

[10] Tweed, J., and Rooke, D. P., "The Elastic Problem for an Infinite Solid Containing a Circular Hole with a Pair of Radial Edge Cracks of Different Lengths," *International Journal of Engineering Science*, Vol. 14, No. 10, 1976, pp. 925–933. doi:10.1016/0020-7225(76)90104-X

[11] Brussat, T. R., "Mode 1 Stress Intensity for a Radial Crack at a Hole with Arbitrary Pressure Distribution," *Engineering Fracture Mechanics*, Vol. 14, No. 1, 1981, pp. 233–235. doi:10.1016/0013-7944(81)90031-X